

Dual-Tube Helmholtz Resonator-Based Triboelectric Nanogenerator for Highly Efficient Harvesting of Acoustic Energy

Hongfa Zhao, Xiu Xiao, Peng Xu, Tiancong Zhao, Liguo Song, Xinxiang Pan, Jianchun Mi, Minyi Xu,* and Zhong Lin Wang*

An acoustic wave is a type of energy that is clean and abundant but almost totally unused because of its very low density. This study investigates a novel dual-tube Helmholtz resonator-based triboelectric nanogenerator (HR-TENG) for highly efficient harvesting of acoustic energy. This HR-TENG is composed of a Helmholtz resonant cavity, a metal film with evenly distributed acoustic holes, and a dielectric soft film with one side ink-printed for electrode. Effects of resonant cavity structure, acoustic conditions, and film tension on the HR-TENG performance are investigated systematically. By coupling the mechanisms of triboelectric nanogenerator and acoustic propagation, a theoretical guideline is provided for improving energy output and broadening the frequency band. Specifically, the present HR-TENG generates the maximum acoustic sensitivity per unit area of $1.23 \text{ VPa}^{-1} \text{ cm}^{-2}$ and the maximum power density per unit sound pressure of $1.82 \text{ WPa}^{-1} \text{ m}^{-2}$, which are higher than the best results from the literature by 60 and 20%, respectively. In addition, the HR-TENG may also serve as a self-powered acoustic sensor.

1. Introduction

With the rapid consumption of global energy, the utilization of new energy is of crucial importance for the development of society and the protection of the ecological environment.^[1,2] Triboelectric nanogenerators can effectively collect low-frequency vibration energy and convert it into electrical energy.^[3–9] These nanogenerators are a milestone in the development of new energy research.^[9,10] Their discovery has provided new ideas for the collection of many forms of environmental energy, such as vibrational energy, wind energy, hydropower, and bioenergy.^[11,12]

A sound wave is a special form of mechanical vibration.^[13] As a clean, abundant, and sustainable form of energy, sound waves are ubiquitously present in our surroundings, including various sounds from human activities, airport construction sites, and transportation. Unfortunately, most sound

wave energy has been wasted because of its very low energy density and the lack of effective technologies for harvesting acoustic energy.^[14,15] Energy harvesters operating on the basis of electromagnetic induction or the piezoelectric effect have been proposed to collect various types of vibrational energy, such as vehicle vibration and human movement.^[16–19] However, their application has encountered severe difficulties in regard to acoustic wave energy. The mechanism of power generation using electromagnetic induction is that the conductor in the magnetic field cuts the magnetic induction line to generate induced currents.^[20] However, due to the small acoustic energy density and the rapid change in sound pressure, effective cutting of the magnetic line under the action of an acoustic wave force is very difficult for conductors.^[21,22] Therefore, using electromagnetic induction to collect acoustic wave energy remains a great challenge. In contrast, piezoelectric materials have good sensitivity to slight disturbances, and most of the previous studies regarding acoustic energy harvesting have concentrated on piezoelectric nanogenerators.^[23] However, thus far, such nanogenerators have been limited by low electrical output performance and high structural complexity.^[24] Therefore, an advanced acoustic energy harvester with high output performance and good practicability must be proposed soon.

H. Zhao, Dr. X. Xiao, P. Xu, T. Zhao, Dr. L. Song,
Prof. X. Pan, Prof. M. Xu
Marine Engineering College
Dalian Maritime University
Dalian 116026, China
E-mail: xuminyi@dlmu.edu.cn

Prof. X. Pan
School of Electronics and Information technology
Guangdong Ocean University
Zhanjiang 524088, China

Prof. J. Mi
College of Engineering
Peking University
Beijing 100871, P. R. China

Prof. Z. L. Wang
Beijing Institute of Nanoenergy and Nanosystems
Chinese Academy of Sciences
Beijing 100085, China

Prof. Z. L. Wang
School of Materials Science and Engineering
Georgia Institute of Technology
Atlanta, GA 30332-0245, USA
E-mail: zlwang@gatech.edu

 The ORCID identification number(s) for the author(s) of this article can be found under <https://doi.org/10.1002/aenm.201902824>.

DOI: 10.1002/aenm.201902824

Triboelectric nanogenerators (TENGs) have shown great potential in vibration energy harvesting and power generation.^[24,25] By using flexible electrode materials, a TENG can be very sensitive to external disturbances, making it a possible candidate for collecting acoustic wave energy. Some efforts have been made to convert acoustic vibration into electricity using TENGs. Yang et al.^[24] reported the first organic thin-film-based TENG for harvesting acoustic energy. By utilizing a Helmholtz resonator, the designed nanogenerator produced an open-circuit voltage of 60.5 V and a short-circuit current of 15.1 μA at the sound pressure level of 110 dB. Cui et al.^[26] developed a mesh-membrane-based TENG that can work stably over a broad bandwidth. Great progress in electrical output was observed, with the maximum open-circuit voltage and short-circuit current reaching 90 V and 450 μA , respectively. Based on this work, Liu et al.^[27] proposed an optimized 3D structure to further improve the performance of the sound-driven TENG. Although the electrical output was enhanced, sound reception was still limited in these energy harvesters due to the divergence of spherical waves in air. More recently, Chen et al.^[28] constructed a TENG integrated with a polymer tube. Low-frequency sound wave energy was successfully absorbed using electrospun polyvinylidene fluoride (PVDF) nanofibers as the vibrating membrane. The TENG could generate an open-circuit voltage of 400 V and a short-circuit current of 175 μA under a sound pressure of 115 dB. As seen from the abovementioned studies, the TENG-based acoustic energy harvesters exhibit superior performance compared to those based on piezoelectric or electromagnetic nanogenerators, which indicates their remarkable potential in acoustic energy capture. However, the previous sound-driven TENGs still exhibit low power output. More importantly, the lack of acoustic energy harvesting theory has hindered the advancement of this technology. The study of

the coupling mechanisms of TENG theory and sound propagation theory can provide guidelines for optimizing the output of acoustic energy harvesters and producing the best output in a specific frequency range.

In this work, we present a dual-tube Helmholtz resonator-based triboelectric nanogenerator (HR-TEG). The HR-TEG is composed of a Helmholtz resonant cavity, an aluminum film with evenly distributed acoustic holes, and an FEP film with a conductive ink-printed electrode. With the propagation of acoustic waves, the FEP film alternatively contacts and separates from the aluminum film, thus generating an electrical output. The output performance of the present HR-TEG is theoretically, numerically, and experimentally analyzed. Compared with the conventional single-tube Helmholtz resonator-based TENG, the dual-tube HR-TEG has a better output performance, with the maximum output voltage increasing by 83%. The output performance of the dual-tube HR-TEG is highly related to the acoustic frequency and sound pressure. The tension force in the FEP film can change the response characteristics of the HR-TEG. Furthermore, by reducing the geometric scale of the resonant cavity, the response frequency of the device can cover more than 500 Hz. The output performance of the HR-TEG is compared with those of earlier reported acoustic energy harvesters, and the results indicate that the present HR-TEG has the highest acoustic sensitivity per unit area and power density per unit sound pressure.

2. Results and Discussion

2.1. Structure and Working Principle of the HR-TEG

Figure 1 shows the structure and working mechanism of the HR-TEG. The HR-TEG consists of a Helmholtz resonant

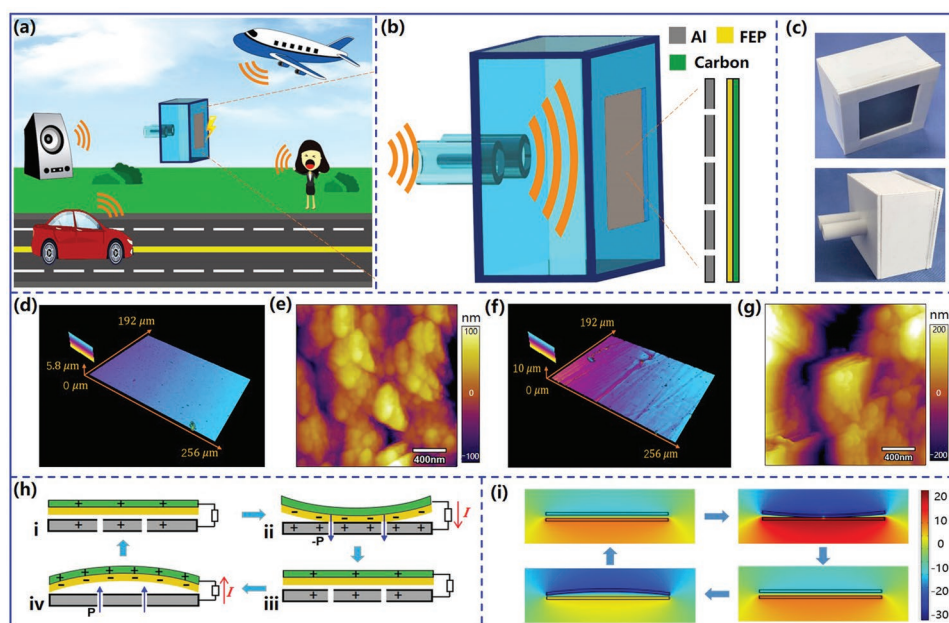


Figure 1. Structure and working principle of the HR-TEG. a) Application background of the HR-TEG. b) Structure scheme of the HR-TEG. c) Two photos of the HR-TEG. d) Laser scanning confocal microscope image of the normal FEP film. e) Surface topography image of the normal FEP film. f) Laser scanning confocal microscope image of the sanded FEP film. g) Surface topography image of the sanded FEP film. h) Working mechanism of the sound-driven HR-TEG. i) COMSOL simulation of the periodic potential change between the two electrodes of the HR-TEG.

cavity, an aluminum film with evenly distributed acoustic holes, and an FEP film with a conductive ink-printed electrode (Figure 1b,c). The Helmholtz resonant cavity is a fundamental acoustic resonance system. It can improve the output performance of the HR-TENG by centralizing the acoustic wave energy and amplifying the sound wave. The FEP material has a strong electronegativity and can generate a large amount of charge transfer during its contact with the aluminum electrode.^[29] Given that the FEP material is insulated, a conductive ink electrode with a micrometer thickness is attached to the back side of the FEP film to transfer electrons. Figure 1d,e shows a laser scanning confocal microscope image and a surface topography image (scanned by an atomic force microscope) of the normal FEP surface. Figure 1f,g shows the sanded FEP surface. The sanded FEP surface is lumpier and has more grooves. The microstructures on the FEP film can greatly increase the contact area and contact stress with the aluminum film during the contact-separation mode, thus improving the output performance of the HR-TENG.^[30] An output performance comparison of the normal and sanded FEP films is shown in detail in Figures S1 and S2 (Supporting Information).

Figure 1h schematically depicts the working mechanism of the HR-TENG. The wave characteristic of sound propagation will induce periodic changes in the pressure between the FEP film and the aluminum film, causing the FEP film to oscillate repeatedly. When the FEP film is in contact with the aluminum film, the electron clouds on the surfaces of the two films overlap, and some of the electrons from the aluminum film enter the deeper potential well of the FEP film.^[29] Due to the much higher electronegativity of FEP than aluminum, the free electrons on the surface of the aluminum film transfer to the lowest unoccupied molecular orbital (LUMO) of the FEP interface.^[30] Namely, the surface of the FEP film becomes negatively charged, while the aluminum film becomes positively charged (Figure 1di). Due to the change in the acoustic pressure difference, the FEP film is separated from the aluminum electrode. Since the negative and positive triboelectric charges no longer coincide on the same plane, a dipole moment and an electrical potential are generated between the two contact surfaces. As a result, free electrons are driven to flow from the conductive ink electrode to the aluminum electrode through an external circuit to balance the local electric field, thereby producing a positive charge on the conductive ink electrode (Figure 1dii). The flow of electrons lasts until the separation of the two contact surfaces is maximized (Figure 1diii). Thereafter, the FEP film is pushed back toward the aluminum film by the action of the sound wave. The potential drop is weakened at this stage, and free electrons in the aluminum film flow back to the conductive ink electrode through the external circuit (Figure 1div). Finally, the two surfaces of the FEP film and the aluminum film come into contact again, with the electrical charge distribution returning to its initial state (Figure 1di). At this point, a full cycle of electricity generation has been completed. Subsequently, the FEP film is separated from the aluminum film again due to the propagation of the sound wave, and another cycle of power generation begins. The working principle of the HR-TENG is further confirmed in Figure 1e, which demonstrates the simulation results of the potential distribution between the two films obtained by

COMSOL software. Thus, an alternating current pulse is generated as the output of the HR-TENG.

2.2. Effect of the Helmholtz Resonator Geometry

The Helmholtz resonator is one of the most-used devices in sound-energy harvesters.^[31] Conventionally, it consists of a sealed chamber and a connection tube. Based on the resonance mechanism of a spring system, the Helmholtz resonator can strengthen the pressure of incident sound and produce a large acoustic pressure magnification. In this part, we present an ultrahigh power density TENG based on a Helmholtz resonant cavity to collect acoustic energy. Enlightened by the structure of the Helmholtz resonator used in silencing systems,^[32] the modified resonator has two connection tubes. Figure 2a shows the geometries of the TENGs with a single tube, with dual tubes, and without a resonator.

To investigate the performance of the HR-TENG in harvesting acoustic energy, a loudspeaker is used to provide sinusoidal sound waves. The frequency of the acoustic source can be regulated by the function signal generator. The experimental process diagram is shown in Figure S3 (Supporting Information). A sound level meter located near the FEP film is used to measure the sound pressure level. The accuracy and resolution of the sound level meter are 1.5 dB and 0.1 dB, respectively. Figure 2b displays the open-circuit voltage of the TENGs with a single tube, with dual tubes, and without a resonator under an acoustic frequency of 100 Hz and a sound pressure level of 79 dB. As expected, the Helmholtz resonator can significantly increase the power output of the TENG. The peak voltage of the TENG without a resonator is only 2.6 V, and this value rises to 7.0 V when the conventional Helmholtz resonator is applied. More notably, the peak output voltage of the HR-TENG with the modified dual-tube resonator can reach up to 20.7 V. This result indicates that, compared to that with a single tube, the Helmholtz resonator with dual tubes can improve the output performance of the TENG by 196%.

The output performances of the resonator-free TENG and the HR-TENGs based on the conventional single-tube Helmholtz resonator and the dual-tube modified Helmholtz resonator are evaluated. Figure 2c shows their peak open-circuit voltages at different acoustic frequencies. With the application of the dual-tube Helmholtz resonator, the electrical output of the HR-TENG is remarkably improved. The maximum open-circuit voltage can reach 27 V at the optimal frequency of 90 Hz, 83% higher than the maximum voltage of the HR-TENG with the conventional resonator. The optimal frequency of the single-tube resonator is 70 Hz. For the acoustic waves with frequencies below this value, the HR-TENGs with the conventional and modified resonators show similar capabilities in harvesting acoustic energy. However, the output voltage of the HR-TENG based on the dual-tube resonator is much higher when the acoustic wave frequency is higher than 70 Hz. A maximum improvement of 198% is reached at an acoustic frequency of 90 Hz. This difference gradually disappears when the frequency exceeds 180 Hz. At its optimal frequency of 190 Hz, the resonator-free TENG has a peak voltage of 8 V. The corresponding output is decreased by 270% when the Helmholtz

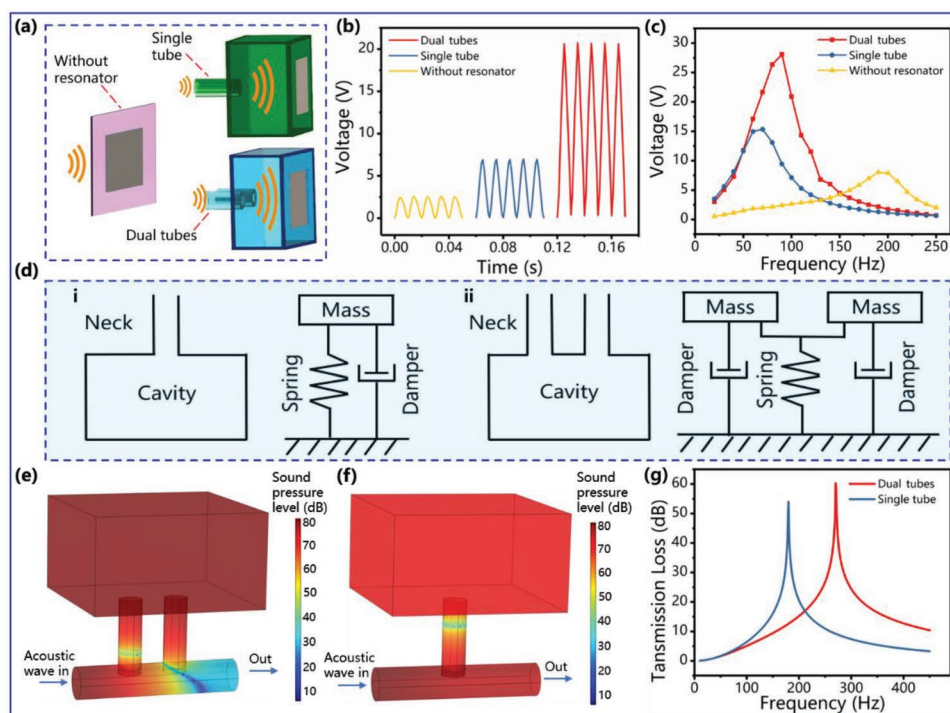


Figure 2. Geometric structure, output performance, and transmission loss of TENGs with a single tube, with dual tubes, and without a resonant cavity. a) Diagrammatic drawing of TENGs with a single-tube resonator, with a dual-tube resonator, and without a resonant cavity. b) Open-circuit voltage of the HR-TENGs under the same acoustic wave condition. c) Open-circuit voltage of the HR-TENGs at different acoustic frequencies. d) Single-tube and dual-tube Helmholtz resonators modeled by mass-spring-damper systems. e, f) Sound pressure level distributions of the dual-tube Helmholtz resonator and single-tube Helmholtz resonator under an acoustic frequency of 280 Hz. g) Comparison of the transmission loss for the single-tube and dual-tube Helmholtz resonant cavities.

resonators are used. Similar results can also be found for the short-circuit current and charge transfer profiles (Figure S4, Supporting Information).

The variation in the optimal output frequency and output performance can be clarified by the changes in the resonant frequency and the acoustic transmission loss (TL). Theoretically, when the incident acoustic wavelength is much larger than the geometric dimension of the resonant cavity, the conventional Helmholtz resonator can be seen as a 1D lumped system.^[33] As shown in Figure 2d,i, the Helmholtz resonator can be modeled as a mass-spring-damper system. The air in the neck oscillates as a mass, and the air inside the cavity expands and contracts like a spring. In addition, the viscous losses due to the friction of the oscillating air in the neck and the radiation losses at the end of the neck can be treated as a damper. The resonant frequency depends on the size of the cavity and the connection tube, and it has the following formulation

$$f = \frac{c}{2\pi} \sqrt{\frac{S}{LV}} \quad (1)$$

where S and L are the cross-sectional area and the effective length of the connection tube, respectively. c is the speed of sound in air, and V is the volume of the resonant cavity. By substituting the geometric values into the above equation, we obtain the resonant frequency of the conventional Helmholtz resonator, which is 184 Hz. The modified dual-tube Helmholtz

resonator can also be modeled as a 1D mass-spring-damper system. To calculate its resonant frequency, the muffler method is used to study the resonance characteristics of the modified Helmholtz resonant cavity based on the modeling framework of COMSOL Multiphysics.^[34] The calculation results when the sound wave frequency is 280 Hz are exhibited in Figure 2d,e. A higher sound pressure in the cavity indicates that a better resonance effect is achieved, and the difference in the sound pressure levels between the inlet and outlet of the horizontal pipe is the transmission loss. The TL is one of the most important evaluation indexes of muffler acoustic performance. Generally, it can be expressed as

$$TL = 20 \lg \left| \frac{P_i}{P_t} \right| \quad (2)$$

where P_i and P_t are the incident sound pressure at the muffler inlet and the transmitted sound pressure at the muffler exit, respectively. Therefore, a higher acoustic wave TL means a better resonant effect of the cavity. The silencing effect of the dual-tube resonant cavity is very significant at this sound wave frequency, while the single-tube resonant cavity has little silencing effect. Furthermore, the overall silencing effects of the single-tube and dual-tube resonant cavities are evaluated for acoustic frequencies ranging from 10 to 500 Hz. Figure 2f shows the acoustic TL curve. The resonant frequency of the single-tube conventional Helmholtz resonator is 184 Hz,

which is consistent with the formula calculation result, and its muffling bandwidth is 16 Hz for a TL of 30 dB. Compared to the conventional resonator, the resonant frequency of the modified dual-tube Helmholtz resonator increases to 270 Hz. More importantly, its resonant frequency band is widened by 88%, and the peak TL is increased by 12%. This result indicates that the HR-TENG based on the modified dual-tube Helmholtz resonator can exhibit a higher electrical output at the resonant frequency and a better output at more acoustic frequencies.

More interestingly, the response frequency of the HR-TENG can be further increased by increasing the resonant frequency of the Helmholtz resonator. According to the calculation theory of the resonator, the resonant frequency can be increased by reducing the cavity size. Thus, a small Helmholtz resonator with a size of 40 mm × 40 mm × 20 mm is used, and the simulation of the resonant frequency is shown in Figure S5 (Supporting Information). The output performance of the new HR-TENG is displayed in Figure S6 (Supporting Information). Apparently, the optimal frequency of the HR-TENG is increased to 350 Hz, and a good electrical output is obtained in the frequency range of 50 to 600 Hz. The diameter of the dual tube is changed from 10 to 7 mm so that the resonant frequency of the dual-tube resonant cavity is the same as that of the single-tube resonant cavity (Figure S7a, Supporting Information). The result is the same as before, and the resonant frequency band of the dual-tube resonator is wider. Therefore, the HR-TENG with the dual-tube resonator is expected to have a better output, and the experimental results confirm this inference (Figure S7b, Supporting Information).

Compared to the single-tube Helmholtz resonator, the dual-tube resonant cavity exhibits a broadened resonant frequency band, i.e., has a high TL over a wider resonant frequency band. Therefore, the TENG with the dual-tube resonator has a better output. At the same time, the dual-tube resonator has a higher resonant frequency, thus increasing the response frequency of the entire system. Therefore, the response frequency of the TENG with the dual-tube resonator is higher than that with the single-tube resonator. Overall, the modified HR-TENG has a better output performance than the conventional Helmholtz resonator-based TENG.

Comparing the theoretical calculation result and the experimental data, the effects of the dual-tube resonator on the variation tendencies of the resonant frequency and the output magnitude have been accurately predicted, but the calculated resonant frequencies for both the conventional and modified resonators are much larger than the experimental results. This discrepancy occurs because the resonant frequency is calculated assuming that the cavity is a sealed chamber and that the electrode film has the same stiffness as the cavity. In fact, the FEP film is an elastic element that oscillates under acoustic wave excitation. Thus, the resonant frequency of the lumped system is shifted. After changing the hard boundary on the top side of the cavity to an elastic boundary, the simulation shows that the resonant frequency of the system is shifted to 80 Hz, in accordance with the experimental results (Figure S8, Supporting Information). At the same time, due to factors of the acoustic conditions and film conditions, the optimal output frequency is near the resonant frequency but does not exactly match it. Therefore, the resonant band of the Helmholtz resonator is

very important. By changing the initial in-plane tension force on the FEP film, the oscillation coupling between the air in the cavity and the FEP film as well as the electrical output will be changed. This result indicates that the tension force has a marked impact on the performance of the Helmholtz resonator-based TENG, which will be discussed in Section 2.4.

2.3. Effect of Acoustic Wave Conditions

To clarify the response of the dual-tube HR-TENG to acoustic waves, the electrical output dependence on the sound pressure and frequency is investigated in this part. An acoustic wave is actually a type of mechanical wave. The mass point that the acoustic wave reaches vibrates near the equilibrium position along the propagation direction. This process is accompanied by energy transfer. Figure 3a shows a schematic diagram of acoustic wave propagation. The sound intensity (I) and sound pressure (P) are the two characteristic parameters that describe the acoustic wave propagation and are defined by the following expressions

$$I = \frac{1}{2} \rho c \omega^2 \varepsilon^2 \quad (3)$$

$$P^2 = I \rho c \quad (4)$$

where ρ is the density of the medium, c is the speed of sound, ω is the angular frequency, and ε is the amplitude of the acoustic wave. As seen from the above formulations, the sound pressure of the acoustic wave is proportional to the square of the acoustic frequency and amplitude. Taking the FEP film of the HR-TENG as the mass body, it reciprocates with the alternating sound pressure, thus generating an electrical output. Figure 3b depicts the relationship between the output voltage of the HR-TENG and applied sound pressure under a certain frequency of 100 Hz. The output voltage evidently increases with the sound pressure. As the sound pressure level increases from 76.7 to 88.4 dB, the peak voltage is increased from 25 to 118 V.

This phenomenon is caused by the coupling mechanism of sound propagation and the TENG. According to Newton's second law, the radial displacement of the FEP film can be expressed as

$$x(t) = \int_0^{\frac{1}{2f}} \left(\int_0^{\frac{1}{2f}} \frac{P S \sin t}{m} dt \right) dt = \int_0^{\frac{1}{2f}} \left(\int_0^{\frac{1}{2f}} \frac{\sqrt{2} \pi f \rho c S \varepsilon \sin t}{m} dt \right) dt \quad (5)$$

where S is the area of the FEP film, m is the film quality, and f is the acoustic wave frequency. Thus, the radial displacement of the FEP film increases with the sound pressure when the frequency is fixed. Furthermore, the HR-TENG operates in the contact-separation mode, and its governing equation can be written as

$$V_{oc} = \frac{\sigma x(t)}{\varepsilon_0} \quad (6)$$

where V_{oc} is the open voltage, σ is the charge density, $x(t)$ is the film displacement, and ε_0 is the dielectric constant. When

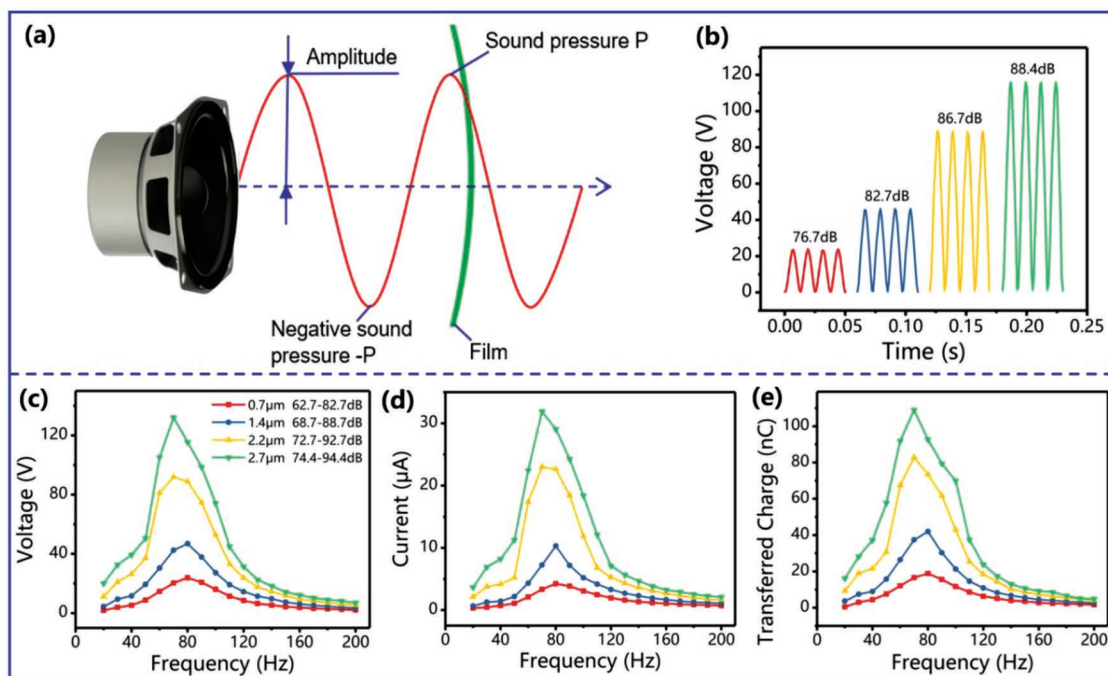


Figure 3. Demonstration of acoustic wave characteristics and electrical output response to sound waves. a) Schematic diagram of acoustic wave propagation. b) Open-circuit voltage of the dual-tube HR-TENG under the excitation of acoustic waves with different sound pressure levels. c) Open-circuit voltage, d) short-circuit current, and e) transferred charge of the dual-tube HR-TENG under the excitation of acoustic waves with frequencies ranging from 20 to 200 Hz.

the acoustic wave frequency is fixed, larger displacement and deformation of the FEP film are expected with an increase in the sound pressure, and thus, a higher output performance is achieved. However, for a fixed acoustic wave amplitude, the effect of the acoustic frequency on the electrical output of the HR-TENG is not unidirectional. As shown in Equations (5) and (6), an increase in the acoustic frequency enlarges the integral variable but simultaneously shortens the integral time. As a result, a peak output voltage exists with increasing acoustic frequency.

A further characterization is carried out to examine the frequency dependence of the HR-TENG's output performance, and the detailed relationship is demonstrated in Figure 3c–e. The acoustic frequency ranges from 20 to 200 Hz, and the sound pressure level spreads from 62.7 to 94.4 dB. With increasing acoustic amplitude, the electrical output is enhanced. At an acoustic frequency of 70 Hz, the open-circuit voltage is increased from 20 to 132 V and the short-circuit current is increased from 3.4 to 32 μA as the acoustic wave amplitude increases from 0.7 to 2.7 μm . This result is consistent with the theoretical results calculated by the formula. More importantly, under the same acoustic wave amplitude, the output performance changes with the sound frequency. For instance, when the wave amplitude is kept constant at 2.7 μm , the maximum output voltage is obtained at the frequency of 70 Hz. The open-circuit voltage, short-circuit current, and transferred charge can reach 132 V, 32 μA , and 109 nC, respectively. At frequencies away from this optimal value, the TENG's electrical output rapidly decreases. Interestingly, the output characteristics of the modified HR-TENG vary with the acoustic wave. Under

the excitation of an acoustic wave with a lower amplitude, the optimal frequency of the HR-TENG is 80 Hz, but this value decreases to 70 Hz when the wave amplitude is increased to 2.7 μm or higher. Details are shown in Figure S9 (Supporting Information). When the FEP film is changed to a larger thickness of 50 μm , the optimal frequency shift rule becomes more obvious.

2.4. Effect of the Tension Force in the Film

As mentioned before, the tension force in the vibrating FEP film has a marked impact on the output performance of the HR-TENG, and a suitable initial value can optimize its electrical output. Figure 4 shows the dependence of the output performance on the tension force. The tension force is applied by a dual-range force sensor, as shown in Figure S10 (Supporting Information). Figure 4a,b shows the sound field distribution in the resonant cavity and the second-order vibration mode of the FEP film. With a tension force of 50 N m^{-1} , the second-order mode occurs at 902.5 Hz, and the fundamental frequency is near zero. These results are similar in that a displacement peak occurs in the middle of the film. Therefore, the vibration mode in the experiment is also the same, which is advantageous for the output of the HR-TENG. The other two modes and sound field distributions are shown in Figure S11 (Supporting Information). The tension force is an important factor affecting the vibration mode. Under different stress states, the film stiffness changes due to the stress-stiffening effect, thus changing the characteristic frequency of the film.^[35] If the tensile force of the

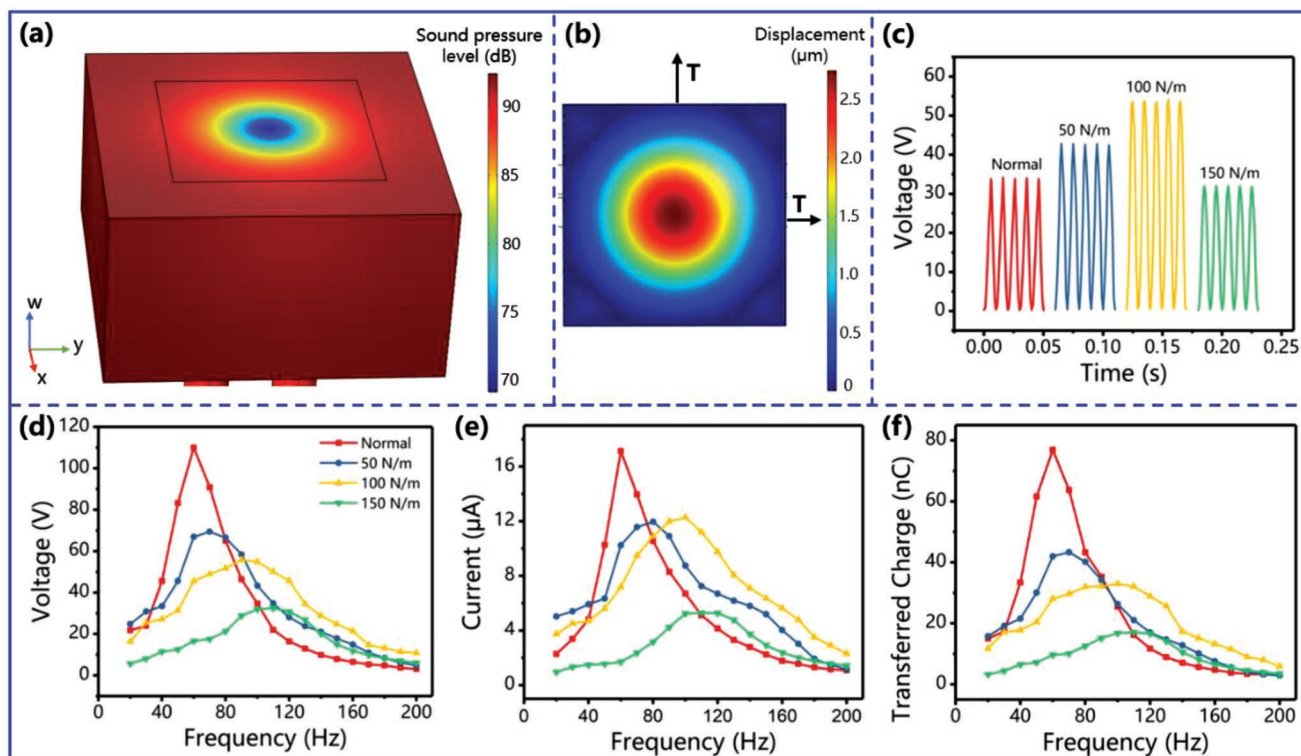


Figure 4. Impact of the tension force in the FEP film on the HR-TENG output performance. a) Sound field distribution in the resonant cavity. b) Second-order vibration mode of the FEP film. c) Open-circuit voltage of the dual-tube HR-TENG with different tension forces under the excitation of a 100 Hz acoustic wave. d) Open-circuit voltage, e) short-circuit current, and f) transferred charge of the dual-tube HR-TENG with different tension forces under the excitation of acoustic waves with frequencies ranging from 20 to 200 Hz.

film increases, its characteristic frequency will also increase. Figure 4c displays the open-circuit voltage of the modified HR-TENG under different tension forces. The excitation acoustic wave has a frequency of 100 Hz and a sound pressure of 84 dB. The peak voltage can reach 34.0, 42.8, 53.7, and 32.0 V. The FEP film with a tension force of 100 N m⁻¹ has the best output under these conditions, which is 1.68 times that with a tension force of 150 N and 1.58 times that for the FEP film without an additional tension force.

Considering that the output performance of the HR-TENG is frequency dependent, an experimental study is conducted under a broad acoustic frequency band to give a full view of the tension force effects. Figure 4c–e presents the open-circuit voltage, short-circuit current, and transferred charge of the modified HR-TENG with different tension forces. The acoustic frequency covers 20 to 200 Hz. In this work, the FEP film that is not subjected to an additional tension force by the force sensor is referred to as the “normal” film. By introducing an initial tension force, the optimal output frequency is increased, and the working bandwidth of the HR-TENG is broadened. When the FEP film is in the normal state, the optimal frequency is 60 Hz, and the electrical output of the HR-TENG is maximized under this condition. The peak values of the open-circuit voltage, short-circuit current, and transferred charge are 110.1 V, 17.1 μA, and 76.9 nC, respectively. With increasing tension force, the optimal frequency increases, and the maximum electrical output gradually decreases. When a 150 N tension force is applied to the FEP film, its optimal frequency is increased

to 110 Hz. The maximum output values are 32.9 V, 5.3 μA, and 17.2 nC, which are 70, 69, and 77% lower than those of the device with the normal film. However, when the acoustic frequency exceeds 80 Hz, the electrical output of the HR-TENG with the normal FEP film sharply decreases, and those devices with tension forces exhibit better performances in collecting acoustic energy, especially that with a tension force of 100 N.

The tension force affects the optimal frequency of the device by changing the vibration mode of the FEP film. Assuming that the FEP film lies in the *x*–*y* plane, it vibrates along the *w* direction. The vibration equation of the rectangular FEP film can be written as

$$T \left(\frac{\partial^2 w}{\partial x^2} + \frac{\partial^2 w}{\partial y^2} \right) = \rho_s \ddot{w} \quad (7)$$

where *w*(*x*, *y*, *t*) represents the displacement of the film at time *t*, *T* is the tension force per unit length, and ρ_s is the areal density. By solving this equation, we obtain the main orthonormal mode and the natural frequency of the FEP film, which are

$$W_{nm}(x, y) = \sin \frac{n\pi}{L_x} x \sin \frac{m\pi}{L_y} y \quad (8)$$

$$f_{nm} = \frac{1}{2} \sqrt{\frac{T}{\rho_s} \left[\left(\frac{n}{L_x} \right)^2 + \left(\frac{m}{L_y} \right)^2 \right]} \quad (9)$$

where L_x and L_y are the lengths of the rectangular FEP film in the x and y directions, respectively. n and m are the modal orders. With increasing tension force, the natural frequency of the FEP film increases, which indicates that the FEP film with a high tension force has a better output performance at high frequencies. The optimal frequency shift rule has the same trend as the characteristic frequency of the film. Therefore, after increasing the tension force of the FEP film, the optimal output frequency is shifted to a larger value. At the same time, the finite element analysis method in COMSOL Multiphysics can be used to simulate the vibration of the FEP film. The TL and vibration modes, which determine the TENG output to a large extent, are calculated and analyzed. Further results can be found in Figure S12 and Note S1 (Supporting Information).

Therefore, regarding the optimized design, the tension force should be determined according to the specific acoustic conditions. To achieve the best output performance of the modified HR-TENG, the normal FEP film should be used when the acoustic frequency is lower than 80 Hz, and a proper tension force should be introduced otherwise.

2.5. Demonstration of the HR-TENG

As an acoustic energy harvester with excellent output performance, the HR-TENG can be utilized to run low power consumption devices. **Figure 5** shows demonstration of the HR-TENG for

acoustic energy harvesting. Under the sound pressure level of 89.1 dB and the acoustic frequency of 80 Hz, the open-circuit voltage, short-circuit current, and transferred charge of the HR-TENG can reach 141 V, 34 μ A, and 122 nC, respectively, as shown in Figure S13 (Supporting Information). The output power is directly supplied to power LEDs. Figure 5a shows the circuit diagram of lighting LEDs, and 464 LEDs are lit simultaneously, as shown in Video S1 (Supporting Information). A demonstration of the HR-TENG charging capacitors with different capacities is plotted in Figure 5b. The AC output from the TENG is applied to both ends of a capacitor via a rectifying bridge, and electric energy is stored in the capacitor. The 47 μ F capacitor is charged from 0 to 3 V under the power supply of the HR-TENG in only approximately 10 s, whereas \approx 208 s are required for the 1000 μ F capacitor to charge from 0 to 3 V, indicating that the HR-TENG has a good charging capability for the capacitors. In addition, a humidity and temperature sensor is also successfully lit up after the 1000 μ F capacitor is charged to \approx 1.5 V. As shown in Figure 5c and Video S2 (Supporting Information), the sensor can work continuously with the power supply of the HR-TENG.

Despite the prevalence of acoustic energy in our surroundings, a major challenge of energy harvesting is its low power density. Micro-electromagnetic generators, piezoelectric nanogenerators, and TENGs are the main devices used in acoustic energy harvesting. The experimental data concerning the output performances of these devices are collected in this paper.^[15,24,26–28,36–41] Their detailed information is presented

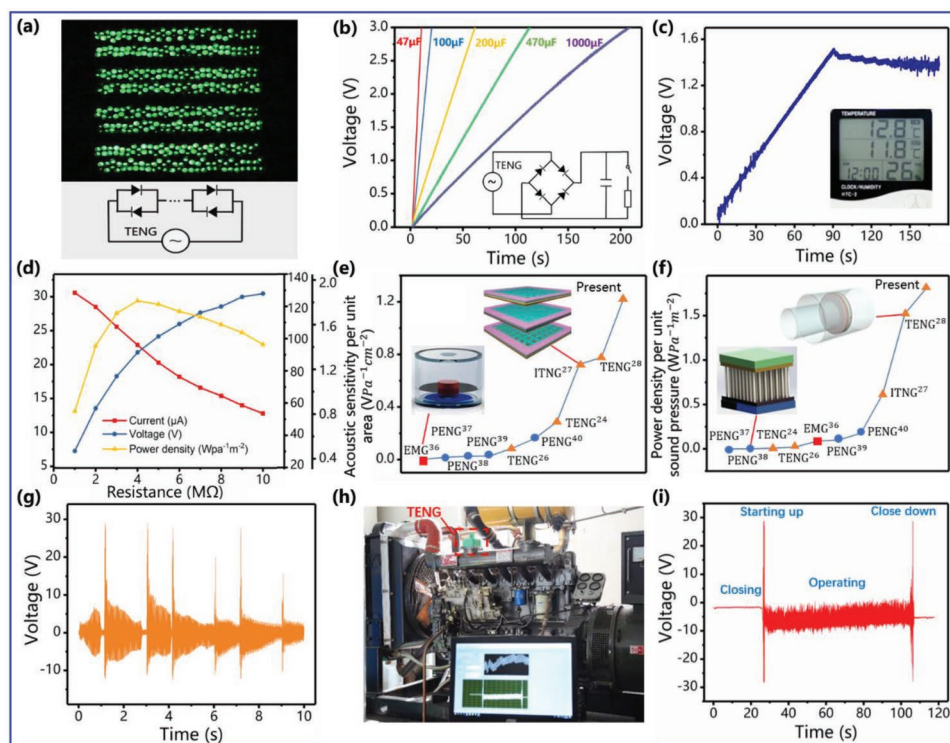


Figure 5. Demonstrations of the HR-TENG as a sustainable power source and for acoustic sensing. a) Photograph of 464 LEDs lit up simultaneously by the HR-TENG and its circuit diagram. b) Charging of capacitors of different capacities by the TENG electrical output and its circuit diagram. c) Experimental graph of the power supply for a temperature and humidity sensor; after the 1000 μ F capacitor is charged to \approx 1.5 V, the sensor works continuously. d) Dependence of the output current, voltage and power density for the HR-TENG on the load resistance. e) Comparison of the acoustic sensitivity and f) power density with those of earlier reported acoustic energy harvesters. g) Voltage waveform of the TENG recording music. h) TENG used to monitor diesel engine operation. i) Voltage waveform diagram of the TENG used to monitor diesel engine vibration.

in Table S1 (Supporting Information). The included acoustic energy harvesters are those with very good output performance for the respective methods.^[33] The comparison results are depicted in Figure 5e,f. As seen from this figure, the acoustic sensitivity of the micro-electromagnetic generator is very low compared to the other acoustic energy harvesters. Because of the low acoustic energy density, movement of the conductor in the electromagnetic generator with the acoustic wave is difficult. Therefore, a sufficient sound pressure is required for the electromagnetic generator to harvest acoustic energy, and its electrical output is small. Piezoelectric materials have a good sensitivity to slight disturbances, and the acoustic sensitivity of the piezoelectric nanogenerators is significantly improved compared to that of the micro-electromagnetic generator. However, the electrical output of the piezoelectric nanogenerators is still low, and the structural complexity has become a challenging issue. TENGs have provided an efficient and cost-effective way to harvest acoustic energy. Overall, the TENGs have very good output performances. Importantly, the sound pressures and areas of the materials used in each work are different and cannot be directly compared. Therefore, the acoustic sensitivity per unit area and power density per unit sound pressure are calculated. The best results from the literature have the acoustic sensitivity per unit area of $0.78 \text{ VPa}^{-1} \text{ cm}^{-2}$ and the power density per unit sound pressure of $1.52 \text{ WPa}^{-1} \text{ m}^{-2}$.^[28] While the present HR-TENG has those of $1.23 \text{ VPa}^{-1} \text{ cm}^{-2}$ and $1.82 \text{ WPa}^{-1} \text{ m}^{-2}$, which are not only much higher than those of the micro-electromagnetic generator and the piezoelectric nanogenerators but also a large improvement over the earlier reported TENGs.

The HR-TENG can also be utilized as a self-powered active sensor. Figure 5g shows the voltage waveform of the TENG recording music. The TENG produces significant voltage changes as the music plays. In addition, upon restoring this voltage waveform back to music by MATLAB (the neural network is shown in Figure S14a, Supporting Information), the restored music is very similar to the original music, as shown in Video S3 (Supporting Information). At the same time, a certain amount of power output can be generated during the recording process, so the TENG can be used as a self-powered recording sensor. Recording of a music waveform for 60 s is shown in Figure S14b (Supporting Information). Furthermore, the HR-TENG can also serve as a self-powered active sensor to monitor diesel engine operation, as shown in Figure 5h. The voltage waveform during the startup, normal operation, and shutdown of the diesel engine is displayed in Figure 5i and Video S4 (Supporting Information). When the diesel engine runs normally, the HR-TENG has a relatively regular and stable output. After the Fourier transform of the voltage waveform, the analysis shows that the main frequency is 50 Hz (Figure S14c, Supporting Information), which is consistent with the diesel piston motion frequency. A sound wave with a large amplitude and a low frequency is projected when the diesel engine is started up or shut down. Accordingly, the TENG produces a large voltage output. Through short-time Fourier transform analysis, the variation process of the first to third main frequencies and the sinusoidal restored waveform from the FFT corresponding to each frequency are obtained, as shown in Figure S15 (Supporting Information). Therefore, in addition

to acoustic energy harvesting, the present HR-TENG has great potential in self-powered sensing.

3. Conclusion

In this work, we presented a dual-tube Helmholtz resonator-based TENG to harvest acoustic energy. The FEP film in the Helmholtz cavity alternatively contacts and separates from the aluminum film under the excitation of an acoustic wave, thus generating an electrical output. Compared to the TENG based on the conventional Helmholtz resonator, the dual-tube HR-TENG has a much better output performance, with the maximum output voltage increasing by 83%. The output dependence on the acoustic frequency and sound pressure has been clarified. When the acoustic wave frequency is fixed, larger displacement and deformation of the FEP film are expected with an increase in the sound pressure, and thus, a higher output performance is achieved. However, for a fixed acoustic wave amplitude, the effect of the acoustic frequency on the electrical output of the HR-TENG is not unidirectional. Thus, a peak output voltage exists with increasing acoustic frequency. Under the optimal output frequency of 70 Hz and sound pressure level of 85.3 dB, the open-circuit voltage and short-circuit current can reach 132 V and 32 μA , respectively. The tension force also has a marked impact on the output performance of the HR-TENG. The optimal frequency shift rule has the same trend as the characteristic frequency of the film. After increasing the tension force of the FEP film, the optimal output frequency is shifted to a larger value. Furthermore, by reducing the geometric size of the resonator, the response frequency of the HR-TENG can reach more than 500 Hz. The output performances of a micro-electromagnetic generator, piezoelectric nanogenerators, and TENGs for acoustic energy harvesting are compared. The TENGs show very good output performances and application potential in the acoustic energy harvesting area. With the optimized design, the HR-TENG can generate a maximum acoustic sensitivity per unit area of $1.23 \text{ VPa}^{-1} \text{ cm}^{-2}$ and a power density per unit sound pressure of $1.82 \text{ WPa}^{-1} \text{ m}^{-2}$, which are higher than the best results from the literature by 60 and 20%, respectively. Furthermore, the HR-TENG has been proven to serve as a self-powered active sensor for acoustic recording and diesel engine operation monitoring. Therefore, this work not only provides effective guidelines for converting acoustic energy into electricity with high efficiency but also presents potential applications of the HR-TENG in acoustic sensing.

4. Experimental Section

Fabrication of the HR-TENG: The HR-TENG consists of a Helmholtz resonant cavity, an aluminum film with acoustic holes, and an FEP film with a conductive ink-printed electrode. The present resonant cavity has a size of $73 \text{ mm} \times 73 \text{ mm} \times 40 \text{ mm}$. One or two tubes with an inner diameter of 5.0 mm and a length of 32 mm were fixed on the resonant cavity. The aluminum film with 440 uniformly distributed acoustic holes acts as the electropositive triboelectric layer. The length, width, and thickness of the film are 45 mm, 45 mm, and 0.1 mm, respectively, and the diameter of the holes is 0.5 mm. The FEP film is used as the electronegative triboelectric

layer due to its strong electronegativity and good flexibility. It has a thickness of 12.5 μm and a working area of 45 mm \times 45 mm. Given that the FEP material is insulated, a conductive ink electrode with a micrometer thickness was attached to the back side of the FEP film to transfer electrons. The shell was printed by a 3D printer with PLA material. The shell can be printed in a variety of shapes and sizes using 3D-printed materials with high precision for the convenience of comparison experiments. The high fill density shell has a smooth surface and good airtightness, which is good for reflection and resonance of sound waves.

Electrical Output Measurements: When measuring the electrical output of the HR-TENG, the device was mounted on an optical plate with a loudspeaker (JBL), which is driven by a sinusoidal wave from a function generator (YE1311). Music was played through the power amplifier (SA-5016). The accuracy and resolution of the sound level meter (GM1353) are 1.5 dB and 0.1 dB, respectively. A dual-range force sensor (Vernier LabQuest Mini) and a data collector (Vernier) were used to measure the tension of the film. The output signals, including the open-circuit voltage, short-circuit current, and transferred charges, were measured by a Keithley 6514 electrometer. Laser confocal microscopy (TCS-SP) was used to scan the surface topography of the FEP film. Atomic force microscopy (Cypher-ES) was used to scan the surface topography and surface potential of the FEP film, and the probe model is ASYELEC-01-R2 (1.42 nN nm⁻¹). The model of the diesel engine used in the experiment is 6105AZLD. A screen printing device (Tou) was used to print the conductive ink (CH-8(MOD2)) on the FEP film (WitLan).

Numerical Simulations: COMSOL Multiphysics was used for simulation calculations. The principle simulation in Section 2.1 of the article uses 2D dimensions, AD/DC modules, current interfaces, and analysis of transient and steady states. The acoustic simulation in Section 2.2 of the paper uses 3D dimensions and a pressure acoustic module to analyze the frequency domain. The acoustic and modal analysis in Section 2.4 of this paper uses 3D dimensions and an acoustic shell interaction module to analyze the frequency domain.

Supporting Information

Supporting Information is available from the Wiley Online Library or from the author.

Acknowledgements

H.Z. and X.X. contributed equally to this work. Support from the National Natural Science Foundation of China (Grant Nos. 51879022, 51979045, and 51906029), the Fundamental Research Funds for the Central Universities, China (Grant Nos. 3132019037, 3132019197, 3132019196, and 3132019331), Projects for Dalian Youth Star of Science and Technology (Grant No. 2018RQ12), the National Key Research and Development Program of China (Grant No. 2016YFA0202704), and the “Thousands Talents” program for pioneer researcher and his innovation team in China are appreciated. Many thanks to Dr. Yi-Cheng Wang for putting forward many valuable suggestions at the beginning of the paper writing.

Conflict of Interest

The authors declare no conflict of interest.

Keywords

acoustic energy, dual-tube Helmholtz resonator, self-powered sensor, triboelectric nanogenerator

Received: August 29, 2019

Revised: October 8, 2019

Published online:

- [1] Q. Schiermeier, J. Tollefson, T. Scully, *Nature* **2008**, 454, 816.
- [2] S. K. Ravi, Z. Yu, D. J. K. Swainsbury, J. Ouyang, M. R. Jones, S. C. Tan, *Adv. Energy Mater.* **2017**, 7, 1601821.
- [3] S. L. Zhang, M. Xu, C. Zhang, Y.-C. Wang, H. Zou, X. He, Z. Wang, Z. L. Wang, *Nano Energy* **2018**, 48, 421.
- [4] Z. L. Wang, *Mater. Today* **2017**, 20, 74.
- [5] M. Xu, S. Wang, S. L. Zhang, W. Ding, P. T. Kien, C. Wang, Z. Li, X. Pan, Z. L. Wang, *Nano Energy* **2019**, 57, 574.
- [6] M. Xu, T. Zhao, C. Wang, S. L. Zhang, Z. Li, X. Pan, Z. L. Wang, *ACS Nano* **2019**, 13, 1932.
- [7] M. Xu, P. Wang, Y.-C. Wang, S. L. Zhang, A. C. Wang, C. Zhang, Z. Wang, X. Pan, Z. L. Wang, *Adv. Energy Mater.* **2018**, 8, 1702432.
- [8] Q. Zheng, Y. Jin, Z. Liu, H. Ouyang, H. Li, B. Shi, W. Jiang, H. Zhang, Z. Li, Z. L. Wang, *ACS Appl. Mater. Interfaces* **2016**, 8, 26697.
- [9] J. Bae, J. Lee, S. Kim, J. Ha, B. S. Lee, Y. Park, C. Choong, J. B. Kim, Z. L. Wang, H. Y. Kim, J. J. Park, U. I. Chung, *Nat. Commun.* **2014**, 5, 4929.
- [10] Z. L. Wang, *ACS Nano* **2013**, 7, 9533.
- [11] Z. L. Wang, T. Jiang, L. Xu, *Nano Energy* **2017**, 39, 9.
- [12] Y. Chen, Y.-C. Wang, Y. Zhang, H. Zou, Z. Lin, G. Zhang, C. Zou, Z. L. Wang, *Adv. Energy Mater.* **2018**, 8, 1802159.
- [13] Y. Wang, Y. Yang, Z. L. Wang, *NPJ Flexible Electron.* **2017**, 1, 10.
- [14] J. G. Gualtieri, J. A. Kosinski, A. Ballato, *IEEE Trans. Ultrason., Ferroelectr. Freq. Control* **1994**, 41, 53.
- [15] F. Xing, C. Jun, Y. Jin, B. Peng, L. Zhaoling, Z. L. Wang, *ACS Nano* **2015**, 9, 4236.
- [16] N. C. Tsai, S. L. Hsu, *Eur. Phys. J. Appl. Phys.* **2012**, 57, 10101.
- [17] A. L. Gyekenyesi, Q. Wang, Y. Zhang, N. X. Sun, J. G. McDaniel, M. L. Wang, *Proc. SPIE* **2012**, 8347.
- [18] P. Pillatsch, E. M. Yeatman, A. S. Holmes, *Sens. Actuators, A* **2014**, 206, 178.
- [19] D.-A. Wang, N.-Z. Liu, *Sens. Actuators, A* **2011**, 167, 449.
- [20] A. R. M. Faisal, C. Hong, G.-S. Chung, *Sens. Actuators, A* **2012**, 182, 106.
- [21] M. Maták, M. Gašparík, P. Šolek, M. Margetin, presented at 12th Int. Conf. Theory of Machines, Mechanisms, Liberec Technical University, Liberec, Czech Republic, September **2017**.
- [22] B. P. Mann, N. D. Sims, *J. Sound Vib.* **2010**, 329, 1348.
- [23] N. Salim, M. F. M. Idros, S. A. M. Al-Junid, A. H. A. Razak, presented at 14th IEEE Student Conf. Research, Development, Kuala Lumpur, Malaysia, December **2017**.
- [24] J. Yang, J. Chen, Y. Liu, W. Yang, Y. Su, Z. L. Wang, *ACS Nano* **2014**, 8, 2649.
- [25] J. Yang, J. Chen, Y. Yang, H. Zhang, W. Yang, P. Bai, Y. Su, Z. L. Wang, *Adv. Energy Mater.* **2014**, 4, 1301322.
- [26] N. Cui, L. Gu, J. Liu, S. Bai, J. Qiu, J. Fu, X. Kou, H. Liu, Y. Qin, Z. L. Wang, *Nano Energy* **2015**, 15, 321.
- [27] J. Liu, N. Cui, L. Gu, X. Chen, S. Bai, Y. Zheng, C. Hu, Y. Qin, *Nanoscale* **2016**, 8, 4938.
- [28] F. Chen, Y. Wu, Z. Ding, X. Xia, S. Li, H. Zheng, C. Diao, G. Yue, Y. Zi, *Nano Energy* **2019**, 56, 241.
- [29] Z. L. Wang, A. C. Wang, *Mater. Today* **2019**, <https://doi.org/10.1016/j.mattod.2019.05.016>.
- [30] J. Wu, X. Wang, H. Li, F. Wang, W. Yang, Y. Hu, *Nano Energy* **2018**, 48, 607.
- [31] S. Noh, H. Lee, B. Choi, *Int. J. Precis. Eng. Manuf.* **2013**, 14, 1629.
- [32] K. Nagaya, Y. Hano, A. Suda, *J. Acoust. Soc. Am.* **2001**, 110, 289.
- [33] M. A. Pillai, E. Deenadayalan, *Int. J. Precis. Eng. Manuf.* **2014**, 15, 949.
- [34] S.-H. Seo, Y.-H. Kim, K.-J. Kim, *J. Mech. Sci. Technol.* **2016**, 30, 653.
- [35] S. F. Muller de Almeida, *AIAA J.* **1999**, 37, 1017.
- [36] F. U. Khan, I. Izhar, *Int. J. Mater. Sci. Eng.* **2013**, 1, 72.
- [37] S. Qi, M. Oudich, Y. Li, B. Assouar, *Appl. Phys. Lett.* **2016**, 108, 263501.
- [38] S. N. Cha, J. S. Seo, S. M. Kim, H. J. Kim, Y. J. Park, S. W. Kim, J. M. Kim, *Adv. Mater.* **2010**, 22, 4726.
- [39] B. Li, J. H. You, Y.-J. Kim, *Smart Mater. Struct.* **2013**, 22, 055013.
- [40] A. Yang, P. Li, Y. Wen, C. Lu, X. Peng, J. Zhang, W. He, *Appl. Phys. Express* **2013**, 6, 127101.
- [41] H. Guo, X. Pu, J. Chen, Y. Meng, M.-H. Yeh, G. Liu, Q. Tang, B. Chen, D. Liu, S. J. S. R. Qi, *Sci. Rob.* **2018**, 3, eaat2516.